Nuclear Engineering and Design 241 (2011) 4409–4419

Contents lists available at ScienceDirect

Nuclear Engineering and Design

journal homepage: www.elsevier.com/locate/nucengdes

Influence of elbow curvature on flow structure at elbow outlet under high Reynolds number condition

A. Ono*, N. Kimura, H. Kamide, A. Tobita

Oarai Research and Development Center, Japan Atomic Energy Agency, Narita 4002, Oarai, Ibaraki 311-1393, Japan

ARTICLE INFO

Article history:
Received 11 March 2010
Received in revised form 10 June 2010
Accepted 12 June 2010

ABSTRACT

In the design of Japan Sodium-cooled Fast Reactor (JSFR), coolant velocity is beyond 9 m/s in the primary hot leg pipe of 1.27 m diameter. The Reynolds number in the piping reaches 4.2×10^7. Moreover, a short-elbow is adopted in the hot leg pipe in order to achieve compact plant layout and to reduce plant construction cost. Therefore, the flow-induced vibration (FIV) arising from the piping geometry may occur in the short-elbow pipe. The FIV is due to the excitation source which is caused by the pressure fluctuation in the pipe. The pressure fluctuation in the pipe is closely related with the velocity fluctuation. As the first step of clarification of the FIV mechanism, it is important to grasp the mechanism of flow fluctuation in the elbow. In this study, water experiments with two types of elbows with different curvature ratios were conducted in order to investigate the interaction between flow separation and the secondary flow due to the elbow curvature. The experiments were conducted with the short-elbow and the long-elbow under $Re = 1.8 \times 10^5$ and 5.4×10^5 conditions. The velocity fields in the elbows were measured using a high-speed Particle Image Velocimetry (PIV). The time-series of axial velocity fields and the cross-section velocity fields obtained by the high-speed PIV measurements revealed the unsteady and complex flow structure in the elbow. The flow separation always occurred in the short-elbow while the flow separation occurred intermittently in the long-elbow case. The circumferential secondary flows in clockwise and counterclockwise directions flowed forward downstream of reattachment point alternately in both elbows.

1. Introduction

A conceptual design study of an advanced sodium-cooled fast reactor named JSFR (Japan Sodium-cooled Fast Reactor) has been conducted in the FaCT (Fast reactor Cycle Technology development) project in Japan (Ichimiya et al., 2007; Kotake et al., 2008). Fig. 1 shows a schematic view of the primary cooling system of the JSFR. The main cooling system of JSFR consists of two loops in order to reduce the plant construction cost while prototype fast reactor of MONJU has three loops. In addition, the thermal output of JSFR is 3600 MWt and much larger than that of MONJU. Therefore, the sodium coolant flow velocity is beyond 9 m/s in the primary hot leg (H/L) of JSFR and the diameter of pipe is approximately 1.3 m. The maximum Reynolds number in the piping reaches 4.2×10^7. The H/L pipe having a 90° elbow with curvature ratio of $r/D = 1.0$, so-called "short-elbow", is adopted to realize a compact layout of the primary cooling system. In sodium-cooled fast reactors, the system pressure is low and thermal stress is major component of load due to the large temperature difference of coolant in transition conditions. Therefore, the thickness of pipe wall in the cooling system is thinner than that in LWRs.

Under such a condition in the cooling system, flow-induced vibration (FIV) is concerned from a view point of the structural integrity of pipings. The pressure fluctuation in the elbow is the sources of FIV excitation force. In general, the pressure fluctuation and the velocity fluctuation are closely related. Thus, the information of the flow field and velocity fluctuation under very high Reynolds number, $Re = 4.2 \times 10^7$, is needed in order to grasp the mechanism of FIV. However it is difficult to conduct an experiment at such the high Reynolds number. Consequently, we must predict the flow structure up to such a high Reynolds number, $Re = 4.2 \times 10^7$ based on available experimental techniques and numerical simulations.

Idelchik (1986) reported that the total resistance coefficients of bends took nearly constant value for more than $Re = 4.0 \times 10^5$. Shiraishi et al. (2006, 2008) reported the flow pattern and dimensionless velocity profile in the elbow were independent of the Reynolds number at least to $Re = 8.0 \times 10^6$. Therefore the flow structures would be similar for Reynolds number from 4.0×10^5 to at least less than 8.0×10^6. As a first step of the above prediction, it is planned to grasp the detail of flow structure and the mechanism of flow fluctuation in the elbow pipe at more than $Re = 4.0 \times 10^5$.

* Corresponding author. Tel.: +81 29 267 4141; fax: +81 29 266 3867.
E-mail address: ono.ayako@jaea.go.jp (A. Ono).

0029-5493/$ – see front matter © 2010 Elsevier B.V. All rights reserved.
doi:10.1016/j.nucengdes.2010.09.026

Nomenclature

D	inner diameter of pipe
r	curvature radius of elbow
U_m	cross-section averaged flow velocity
γ	forward flow fraction
λ	wavelength
Δi_n	grid size of cross-sectional paper on the captured image
Δr_n	grid size of cross-sectional paper
Δt	time interval of double pulses
x	axial direction downstream the elbow
y	direction from the inside to outside of the elbow
z	vertical direction to x and y
RMS	root mean square value

However, it is not easy to grasp the complex and unsteady flow structure in the elbow, where the separation flow and secondary flow due to the elbow curvature interact with each other.

Many studies on the fluid flow in the pipe with bend or elbow have been conducted. The most of them focused on pressure loss between inlet and outlet of the elbow and time-averaged velocity profile from a view point of industrial application. Some studies were conducted on flow characteristics in the pipe with a 90° bend or an elbow of circular cross-section.

Bovendeerd et al. (1987) measured the velocity fields in a 90° bend with curvature ratio, $r/D = 3$, at $Re = 700$ using the Laser-Doppler Velocimetry (LDV). They choose oil and kerosene as a working fluid in order to match the refractive index of fluid to that of bend material (Perspex). They obtained the time-averaged axial and secondary flow velocities. Enayet et al. (1982) measured the velocity and turbulent intensity fields in a 90° bend pipe with $r/D = 2.8$ at the $Re = 500$, 1093 and 4.3×10^4 using the LDV. Their working fluid was water and refractive index matching technique at the fluid-wall interface was not used. The displacement of the laser measurement volume due to refraction is allowed for simple geometrical calculation. Sudou and Hibara (1992) measured three components of mean and fluctuating velocities in a 90° bend pipe with $r/D = 2$ at a $Re = 6 \times 10^4$ using the hot wire probes. Their working fluid was air.

The flow separation did not seem to occur in the experiments in above studies because of large elbow curvature ratio. In other words, the complex flow structure interacting between the flow separation and secondary flow was not investigated. In JSFR, it is needed to clarify the mechanism of flow fluctuation inducing the FIV, when flow separation occurs in the short-elbow geometry.

Kawamura et al. (2002) measured the velocity field and turbulence intensity field in a 90° elbow with $r/D = 0.55$, 1 and 2 at the $Re = 5 \times 10^4$ and 5×10^5 using LDV measurement. They focused on the turbulent intensity and the characteristics of the power spectrum of the turbulent intensity. They gave the important findings that the normalized power spectrum of the turbulent intensity was not affected by the Reynolds number. Though the separation occurred in the case of $r/D = 0.55$ and 1, the unsteady flow structure formed by the separation and the secondary flow was not mentioned in detail. Shiraishi et al. (2006, 2008) measured the pressure fluctuation and observed the flow regime in the pipe with elbow with $r/D = 1$ up to the $Re = 8.0 \times 10^6$. Although they concluded that the fluctuating pressure was generated by the movement of the boundary of flow separation and reattachment region, their data of axial velocity profile in the elbow measured by LDV was limited at several position and not enough to understand clearly the complex and unsteady flow field around the flow separation region.

In this study, water experiments using the 1/8 scaled elbows were conducted in order to investigate the mechanism of flow fluctuation induced by interaction between the flow separation and secondary flow due to the elbow curvature. The elbow curvature ratio was chosen as an experimental parameter in order to change the intensity of the secondary flow induced by the centrifugal force. The time-series of velocity fields in the elbows were measured using a high-speed Particle Image Velocimetry (PIV).

2. Experiment

2.1. Test loop and test section

Fig. 2 shows the schematic of the experimental test loop with the elbow. Water was used as working fluid. The test section

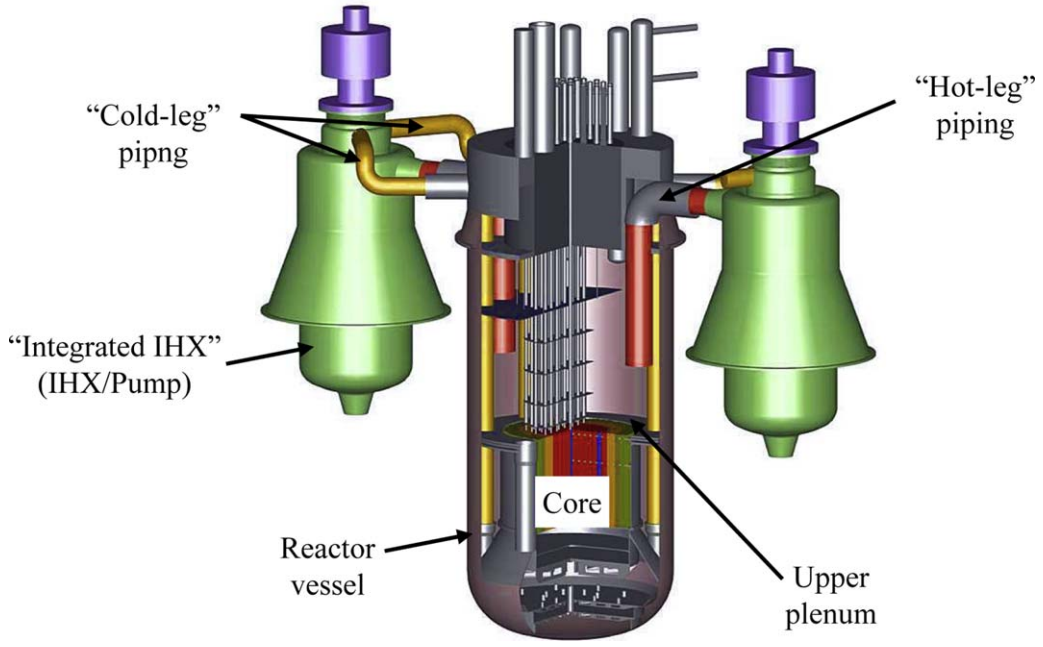

Fig. 1. Schematic view of primary cooling system of the JSFR (Ichimiya et al., 2007; Kotake et al., 2008).

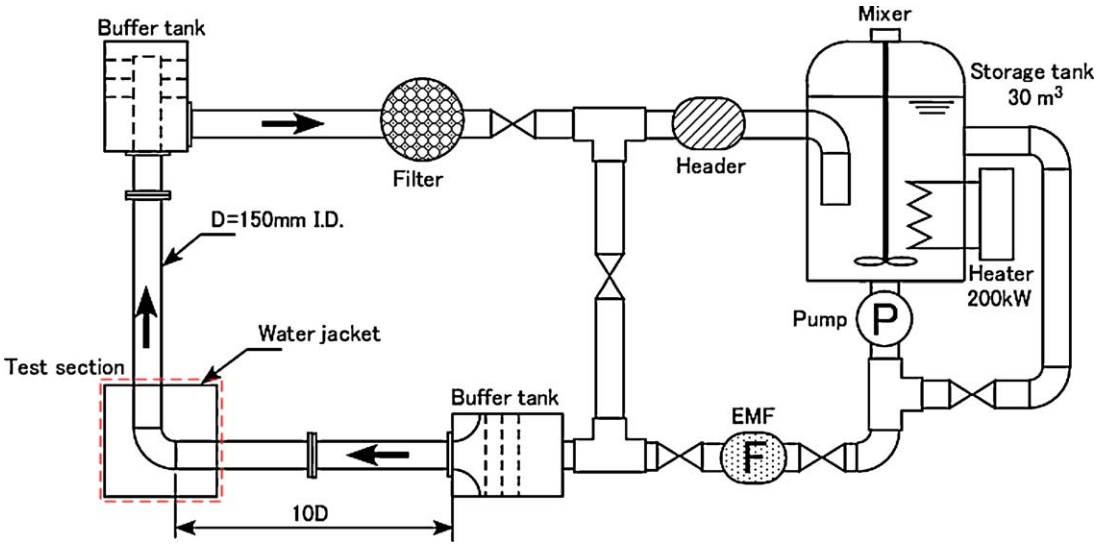

Fig. 2. Schematic of the experimental test loop.

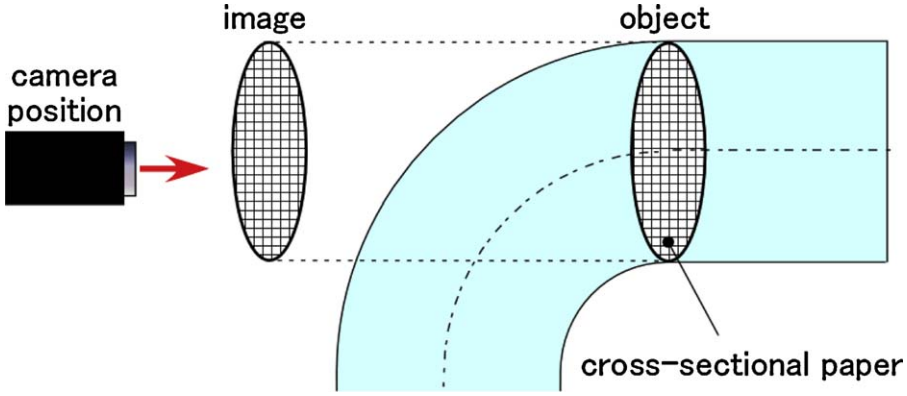

Fig. 3. Evaluation of the optic distortion of the poly-urethan resin elbows.

is composed of the elbow made of the poly-urethane resin and straight pipes made of acrylic resin. The inner diameter of pipe is 150 mm, which is 1/8 scaled model of the H/L pipe in JSFR. The water storage tank contains 30 m^3. Five units of heaters in the tank enable to control the water temperature in the test loop. The total power of heaters is 200 kW. The maximum temperature of water is 50 °C. The maximum flow rate in the test loop is 240 m^3/h. The buffer tank to obtain a flat velocity profile is set on the entrance of the test section. The buffer tank is composed of three baffle plates and a vena contracta nozzle. The distance between the elbow and the inlet buffer tank is nearly 10 times of the diameter of the pipe. In JSFR, the length of H/L pipe connected the short-elbow is nearly 5.7 times of the pipe diameter from the H/L intake.

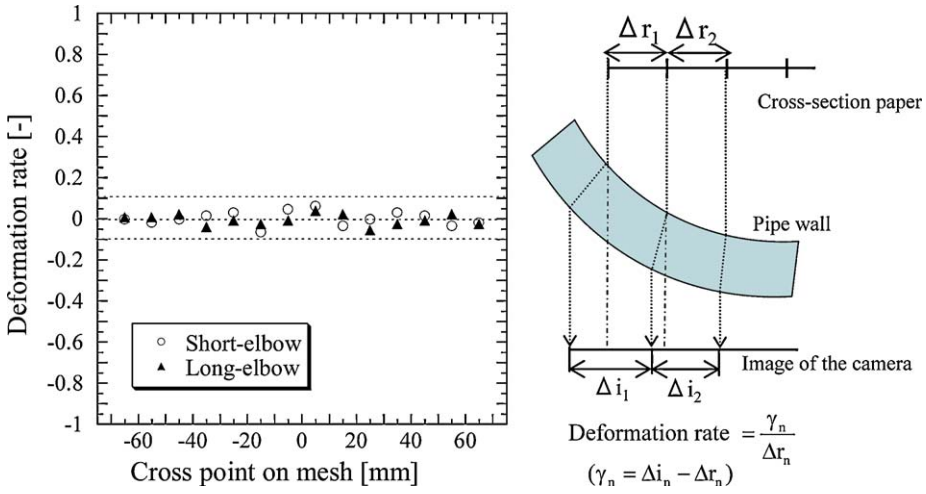

Fig. 4. Deformation rate at cross-section of the pipe.

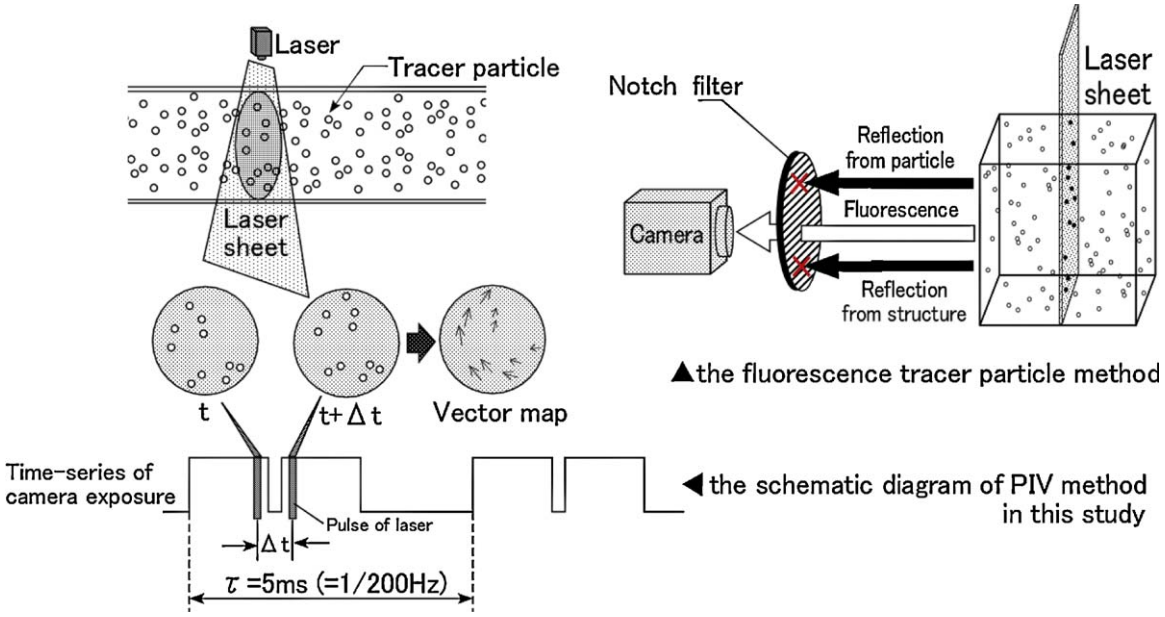

Fig. 5. Schematic diagram of PIV method.

The two types of elbow, $r/D = 1.0$ and 1.5, were used to investigate the influence of the elbow curvature. In general, the elbow with $r/D = 1.0$ is called "short-elbow" and the elbow with $r/D = 1.5$ is called "long-elbow". The visualization of the flow in a round pipe is difficult to keep the measurement precision because of distortion near the wall of pipe. It is important to reduce the influence of optical distortion on captured image for PIV method. So, the seamless elbows made of poly-urethane resin using the technique of casting were applied to the test section in order to avoid the optical distortion on the seam. Moreover the pipe wall of the elbows is very thin, $t = 3$ mm, and a water jacket was set in order to reduce the optic refraction at the wall of the elbow. These efforts greatly reduced the optic refraction near the wall of the elbow.

The optic distortion of our poly-urethane resin elbow was evaluated as follows; the cross-sectional paper put in the elbow was captured by the camera from outside of the elbow as shown in Fig. 3. Fig. 4 shows the deformation rate over the cross-section of pipe calculated from the grid point of captured image. The deformation rate is defined as follows;

$$\text{Deformation rate} = \frac{\gamma_n}{\Delta r_n}, \tag{1}$$

$$\gamma_n = \Delta i_n - \Delta r_n. \tag{2}$$

Here, Δr_n is grid size of cross-sectional paper and Δi_n is grid size of cross-sectional paper on the captured image. The captured image slightly distorted around the center of pipe, where two casts are bonded each other. However, it was found that the influence of refraction was small near the pipe wall even though the elbow had the strong curvature wall.

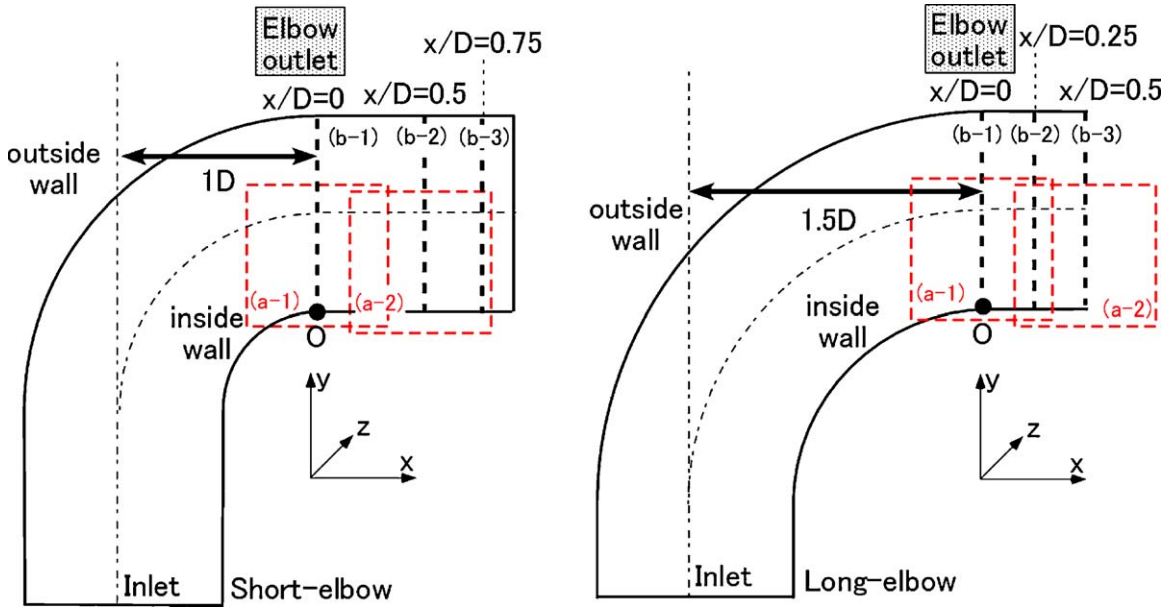

Fig. 6. Position of measurements.

Table 1
Experimental conditions.

Case name	Mean flow velocity, *Um* [m/s]	Temperature [°C]	Re number [–]
Short-elbow			
Low velocity case	1.0	28	1.8×10^5
High velocity case	3.0	28	5.4×10^5
Long-elbow			
High velocity case	3.0	28	5.4×10^5
Low velocity case	1.0	28	1.8×10^5

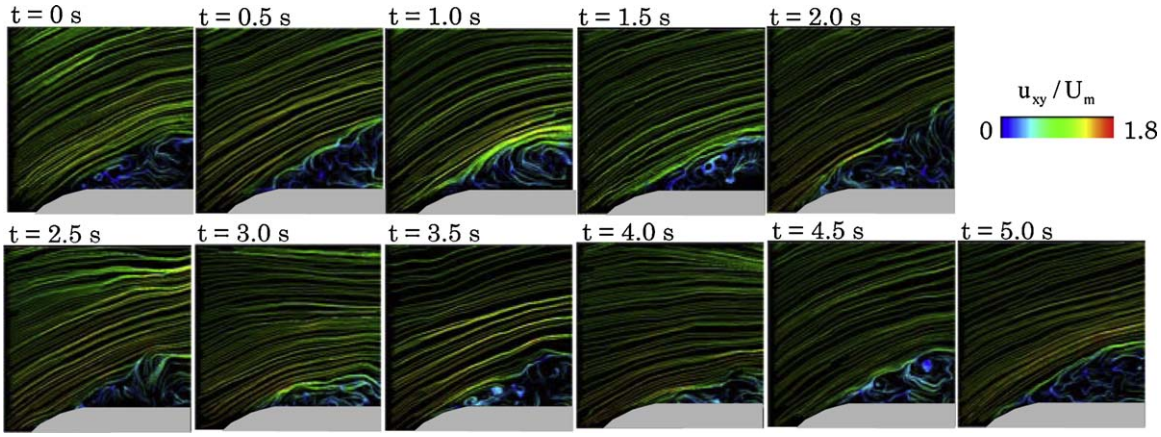

Fig. 7. Time-series of typical flow field in the short-elbow (high velocity case).

2.2. The method of velocity field measurement in the pipes

The flow structure in the elbow is very complex since the secondary flow due to the elbow curvature interacts with the separation flow generated near the inside wall of the elbow. It is important to measure the velocity fields (at least two-dimensional) simultaneously with high time resolution so as to grasp the unsteady complex flow structure in the elbow. The Particle Image Velocimetry (PIV) enables to acquire the time-series of two-dimensional velocity field. In this study, the high-speed PIV was adopted for measuring velocity fields in the pipe.

Fig. 5 shows the schematic diagram of PIV method. The PIV system consisted of an YLF laser, a high-speed camera "Photoron - APX" and a timing controller. In the PIV method, the images of tracer particles lightened by the laser in working fluid are captured as the successive two frames by the high-speed camera. The rapid motion of the tracer particles is captured by the high-speed camera with the high cycle pulse laser method. In this experiment, the time intervals between two laser pulses, Δt, were set from 0.2 ms to 0.5 ms depending on the velocity of main flow. The successive two frames were captured by $\tau = 5$ ms (200 Hz). The total number of frames per one record was 2048, so the number of vector map obtained was 1024 with interval of 5 ms. Therefore, the total time length of record was 5.12 s. The records of image were conducted three times at each measurement position to increase statistical accuracy. The image sizes were 160 mm × 160 mm (1024 pixel × 1024 pixel) and 110 mm × 110 mm (1024 pixel × 1024 pixel). The cross-correlation and sub-pixel methods were used for the PIV data analysis. The reference region was 30 pixel × 30 pixel and the spatial error of the correlation was nearly 0.2 pixel by using the sub-pixel method (Sakakibara et al., 1992). The estimated velocity measurement errors were less than 0.020 m/s and 0.150 m/s in the cases where the intervals of laser emission were 1.5 ms and 0.2 ms, respectively.

It is difficult to measure the velocity near the wall with high precision, since not only the particle images but also the reflection lights from the wall of pipes (halation) are recorded by the camera.

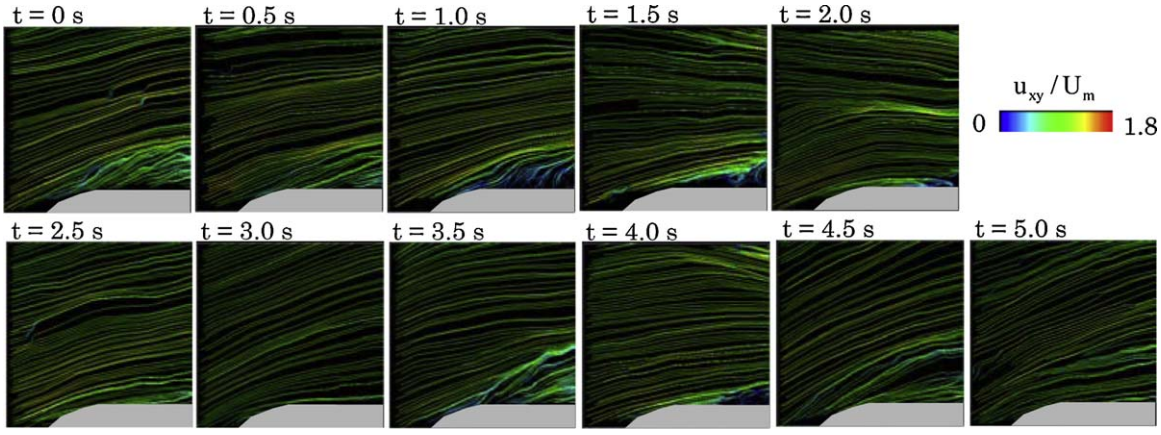

Fig. 8. Time-series of typical flow field in the long-elbow (high velocity case).

In this experiment, the particle which yields fluorescence against light wavelength of laser was adopted as the seeding particle. The optical sharp-edged band-cut filter which cuts off the wavelength corresponding to laser ($\lambda = 527$ nm) was set in front of the camera lens in order to cut the light of reflection from the wall. This "fluorescence tracer particle method" enabled to measure velocity near the wall with high precision by eliminating halation. The fluorescing tracer particle used in this experiment was ion-exchange resin (around 80 μm in diameter) dyed by Rhodamine-640 as fluorescence material.

2.3. The position of measurement

Fig. 6 shows the velocity measurement positions in the experiment. Here, "elbow outlet" is defined as the termination point of curvature in downstream side of the elbow. In the case of short-elbow, the elbow outlet position is the line 1D from the centerline of inlet pipe. In the case of long-elbow, the elbow outlet is the line 1.5D from the centerline of inlet pipe. It is defined that the axial direction downstream the elbow is x-coordinate, the direction from the inside to outside of the elbow is y-coordinate and the perpendicular direction to x and y is z-coordinate. The point on the wall at the elbow outlet is defined as the coordinate origin, $x/D = 0$, $y/D = 0$ and $z/D = 0$. The x–y cross-sections near the inside wall of pipe, (a-1) and (a-2) (see Fig. 6), were captured in order to observe the flow separation. In the short-elbow and the long-elbow, an image was captured with aiming at the elbow outlet line as the image center, (a-1)-section, and another image was captured at 71 mm downstream as the (a-2)-section. The images at the y–z cross-section (b), which were the cross-sections of the pipe, were captured in order to observe the secondary flow. In the short-elbow, images were captured at $x/D = 0$, 0.5 and 0.75. In the long-elbow, images were captured at $x/D = 0$, 0.25 and 0.5. The image sizes were 110 mm × 110 mm (1024 pixel × 1024 pixel) at the section (a) and 160 mm × 160 mm (1024 pixel × 1024 pixel) at the section (b).

2.4. Experimental conditions

Idelchik (1986) arranged the previous data of total resistance coefficients of bends and divided them into three regimes: the sub-critical ($Re < 1 \times 10^5$), transition ($1 \times 10^5 < Re < 4 \times 10^5$) and post-critical ($4 \times 10^5 < Re$) regimes. Starting with very small value of the Reynolds number, the coefficients of total resistance of the bend tend to drop in the sub-critical regime. Following this, the coefficients decrease as Reynolds number increases in the transition regime, and take nearly constant values in post-critical regimes. Shiraishi et al. (2006, 2008) measured the velocity profile in the 90° short-elbow up to $Re = 8.0 \times 10^6$ in the post-critical by using LDV. They found that the flow pattern and the dimensionless velocity distribution in the elbow were independent of the Reynolds number in a region of $4 \times 10^5 < Re < 8.0 \times 10^6$ in the post-critical regime. They explained the reason why the flow resistance coefficient was constant in the post-critical regime as follows: the starting point of separation was rigid at certain location on the wall in the post-critical regime. In other words, the separation formation was independent of Reynolds number up to at least $Re = 8.0 \times 10^6$.

Therefore, it is important to clarify the flow structure in post-critical region in order to predict the flow regime at $Re = 4.2 \times 10^7$ in JSFR. There were a few studies focused on the mechanism of the fluid fluctuation and pressure fluctuation at the high Reynolds number in the post-critical regime. In this study, several experiments were conducted in post-critical regime in order to investigate the flow mechanism under the high Reynolds number condition, and in the transition regime for the comparisons with previous findings under the relatively low Reynolds number condition.

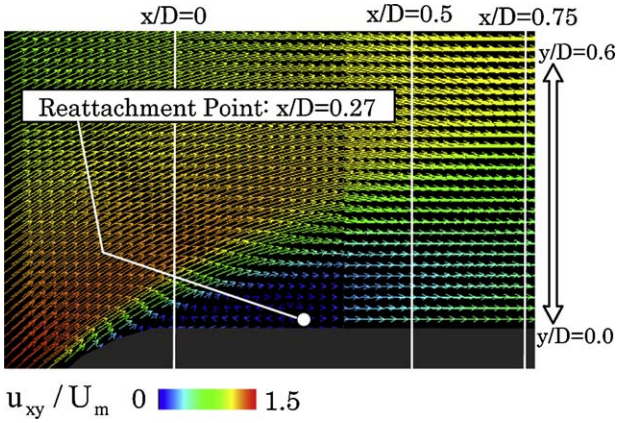

Fig. 9. Time-averaged velocity field near the inside wall in the short-elbow (high velocity case).

Table 1 shows the experimental condition in this study. The test parameter is the cross-section averaged flow velocity, U_m, in the pipe. The low velocity case in the transition regime, $U_m = 1$ m/s, and the high velocity case in post-critical regime, $U_m = 3$ m/s, were conducted in both the short-elbow and the long-elbow cases. The fluid temperature was 28 °C in all cases. Reynolds number is 1.8×10^5 in the low velocity case and 5.4×10^5 in the high velocity case.

3. Results and discussion

3.1. Unsteady flow structure

Figs. 7 and 8 show the time-series of typical flow fields on (a-1)-section in the short-elbow and the long-elbow in the high velocity case, $U_m = 3$ m/s. The velocity was normalized by the mean flow velocity, U_m. The center of each image corresponds to the elbow outlet, $x/D = 0$. At the inside wall in the short-elbow, a low velocity region was observed, where the flow pattern was unsteady and complex. It was found that the flow separation occurred near the inside wall in the short-elbow. This separation region moved up and down periodically and did not disappear all the time. And this movement of separation region seems to give the periodic fluctuation to the velocity field at the downstream region of elbow outlet. At the inside wall of the long-elbow, the steady separation region as seen in the short-elbow was not observed. However, a small separation region appeared intermittently as seen at 1.0 s (see Fig. 8). It was found that the separation region was formed intermittently in the long-elbow.

3.2. The flow structure near the inside wall at the elbow outlet

Figs. 9 and 10 show the time-averaged velocity fields under the high velocity condition near the inside wall in the short-elbow and the long-elbow, respectively. The low velocity region near the inside wall of pipe was seen clearly in the short-elbow case in Fig. 9. It means that the flow separation region was formed constantly near the inside wall in the short-elbow. Fig. 11 shows the distribution of a forward flow fraction, γ, at $y/D = 0.01$ near the inside wall in the short-elbow. The forward flow fraction is defined as the time fraction of the positive velocity component in the main flow direction against the total measurement time. In general, the reattachment point of separation region is defined as the position where the forward flow fraction is 0.5 (Eaton et al., 1979; Sandborn, 1979). According to this definition, the reattachment point was $x/D = 0.1$ in the low velocity case (the transition region) and $x/D = 0.27$ in the high velocity case (the post-critical region). It means that the separation region in high velocity case is formed fur-

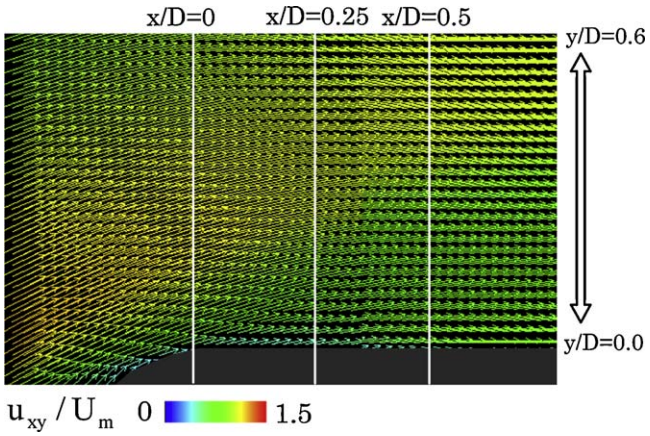

Fig. 10. Time-averaged velocity field near the inside wall in the long-elbow (high velocity case).

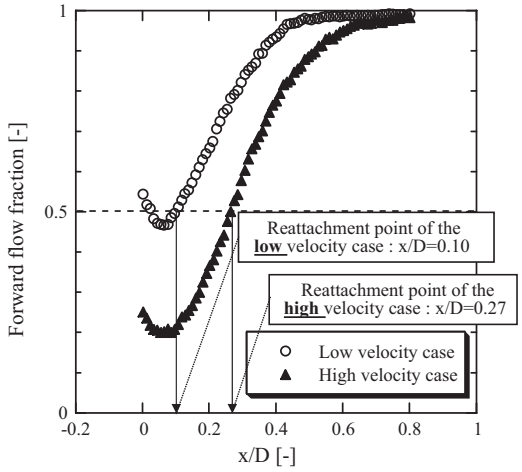

Fig. 11. Distribution of forward flow fraction at height of $y/D = 0.01$ in the short-elbow.

ther downstream side than in low velocity case. This experimental result was consistent with that of Idelchik (1986), i.e., the separation region in the transition regime was formed more upstream than in the post-critical regime. Even though Fig. 10 shows that the separation region was not formed clearly near the inside wall in the long-elbow, the separation phenomena occurred intermittently according to the observation of the time-series flow pattern in Fig. 8. The region near the wall where the velocity is lower than mean velocity corresponds to the separation region appearing intermittently. However, the reattachment point in the long-elbow could not be obtained from the distribution of forward flow fraction since the separation region was not always formed.

Kawamura et al. (2002) measured the turbulent intensities in 90° elbows of $r/D = 0.55$, 1 and 2 using a Laser-Doppler Velocimeter (LDV) and reported that the separation regions with larger curvature ratio were formed more upstream side against the elbow outlet at $Re = 5 \times 10^5$. They also reported that the separation region was not formed in the case of $r/D = 2$ even though it was formed in the case of $r/D = 0.55$ and 1. So, our experimental data were consistent with the experimental results of Kawamura et al.

Figs. 12 and 13 show the time-averaged velocity components in the streamwise direction, u_x, in the short-elbow and the long-elbow, respectively. The vertical axis indicates the dimensionless distance from the inside wall of the elbow. The horizontal axis is the dimensionless velocity normalized by the mean velocity, u_x/U_m. The one-dimensional velocity profiles were plotted every 20 mm from the elbow outlet, $x/D = 0$, to downstream position, $x/D = 0.8$. According to Fig. 12(a), the reverse flow was observed near the inside wall in both the low and high velocity cases. The velocity profiles in the two velocity cases were different from each other. This difference is related to the difference of start point of the separation region. The reattachment points defined by the forward flow fraction were $x/D = 0.1$ in the low velocity case and $x/D = 0.27$ in the high velocity case. So, the reattachment points were located in between (a) and (b) in the low velocity case and at (c) in the high velocity case, respectively. It was found that the velocity near the inside wall was locally accelerated in downstream region from the reattachment point in the short-elbow. In the long-elbow case, Fig. 13 shows that the reverse flow was not observed near the inside wall, and the velocity profiles in both velocity cases nearly agreed at the downstream from $x/D = 0.4$. The axial velocity was slightly accelerated near the wall downstream of elbow outlet as well as in the short-elbow case.

Shiraishi et al. (2006, 2008) also observed this local acceleration phenomenon in a short-elbow by using LDV. They called this phenomenon near the inside wall as "jet" and suggested that "jet" was caused by the convergence of two flows which bypassed the separation region. Tanaka et al. (2009) reproduced such a local acceleration phenomenon in a short-elbow in their numerical simulation and they pointed out that this local acceleration

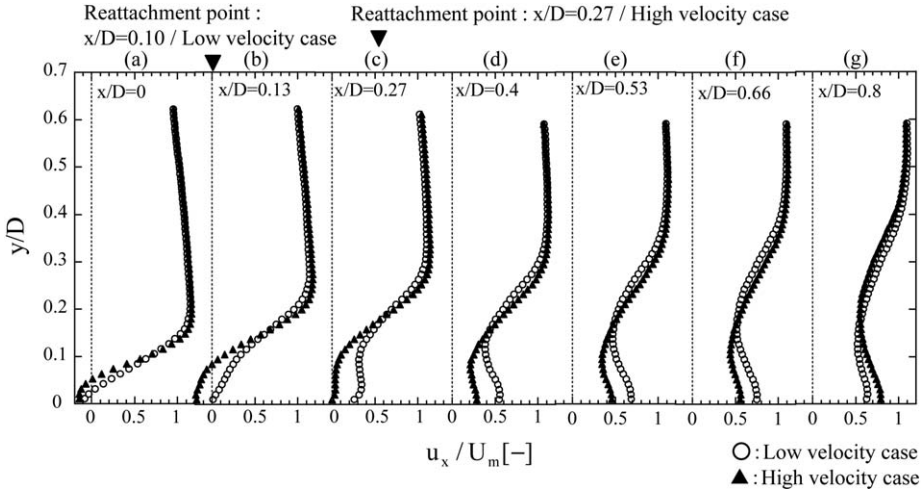

Fig. 12. Transverse distributions of velocity component in the streamwise direction in the short-elbow.

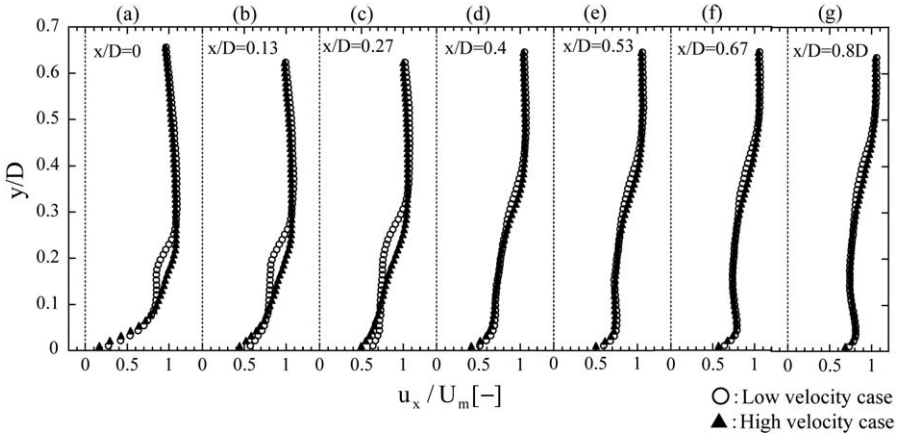

Fig. 13. Transverse distributions of velocity component in the streamwise direction in the long-elbow.

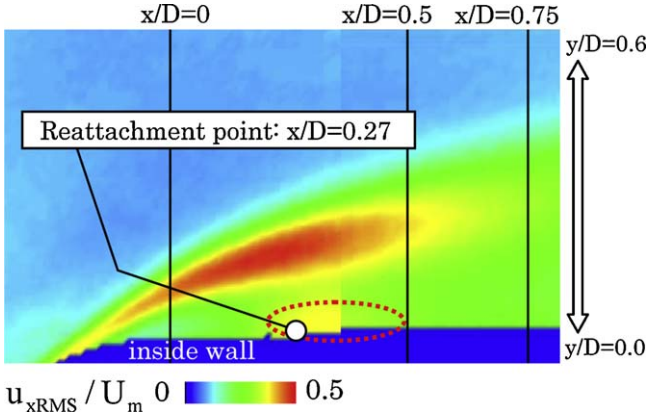

Fig. 14. Contour of the turbulence intensity in the *x*-direction at the short-elbow outlet (high velocity case).

phenomenon was owing to the collision of the circumferential secondary flow at the inside wall.

Figs. 14 and 15 show the contours of the turbulence intensity of the axial velocity, u_x, in the short-elbow and long-elbow in the high velocity cases. The turbulence intensity of $u_{x\mathrm{RMS}}$ is defined as:

$$u_{x\mathrm{RMS}} = \sqrt{\frac{\sum_{i=1}^{N}(u_{xi} - \bar{u}_x)^2}{N}}, \tag{3}$$

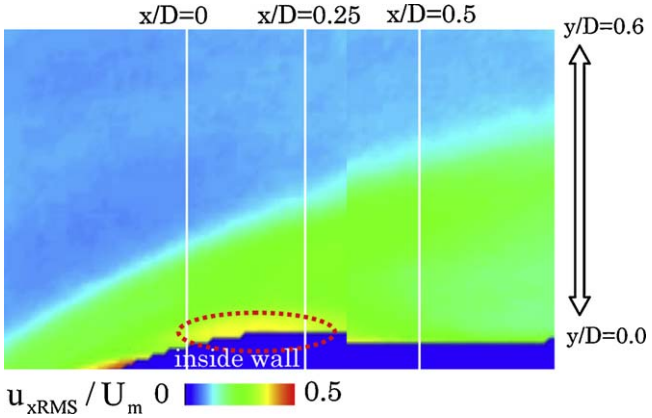

Fig. 15. Contour of the turbulence intensity in the *x*-direction at the long-elbow outlet (high velocity case).

$$\bar{u}_x = \frac{\sum_{i=1}^{N} u_{xi}}{N}. \tag{4}$$

In figures, the turbulent intensity was normalized by the mean velocity. In the short-elbow case, the high turbulence intensity region was observed at the shear layer above the separation region. However, in the long-elbow, the high turbulence intensity at the shear layer was not observed since the separation region was not formed constantly. The other high turbulence intensity region was observed near the inside wall in both the long-elbow and the short-elbow. In the short-elbow case, it is suggested that the high turbulent intensity region near the wall was formed due to the turbulent flow generated by the movement of separation region since the reattachment point located in the front of the high turbulent intensity region. Also in the long-elbow case, it is suggested that the high turbulent intensity region near the wall is formed due to the movement of separation region formed intermittently. In the long-elbow case, even though the reattachment point could not be defined from the distribution of forward flow fraction, it was guessed the reattachment point appearing intermittently in the long-elbow would exist at upstream of high turbulent intensity region, i.e., at the elbow outlet, $x/D = 0$.

Above mentioned, it is found that the very complex fluid structure is formed the downstream of reattachment point due to the flow fluctuation induced by the movement of the separation region and the acceleration phenomenon of axial velocity. Shiraishi et al. (2006, 2008) reported that the large pressure fluctuation was detected around the reattachment point in their experimental work. Therefore, it is important to focus the characteristics of velocity fluctuation near the reattachment point for the clarification of FIV mechanism. In the next section, we discuss how the secondary flow due to the elbow curvature influences the complex flow structure downstream of reattachment point.

3.3. *Influence of secondary flow on the flow structure near the inside wall of the elbow*

Figs. 16 and 17 show the time-averaged velocity fields in the pipe cross-sections at $x/D = 0$, 0.5 and 0.75 in the short-elbow, and $x/D = 0$, 0.25 and 0.5 in the long-elbow in the high velocity cases. The velocity was normalized by the mean velocity. The top of each figure is the outside of the elbow and the bottom is inside of the elbow (see Fig. 6). In the cross-section at $x/D = 0$ of Fig. 16, the strong flow from inside to outside was observed. This corresponds to the main flow which had high axial velocity above the separation region. In the cross-section at $x/D = 0.5$ and 0.75, the circumferential flows in clockwise and counterclockwise directions

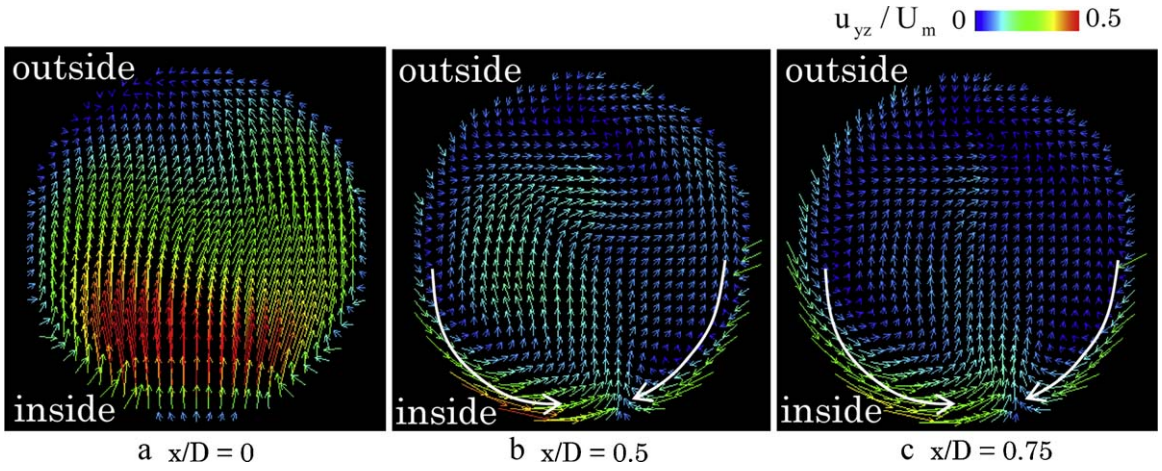

Fig. 16. Time-averaged velocity fields in the cross-section of the pipe (short-elbow case).

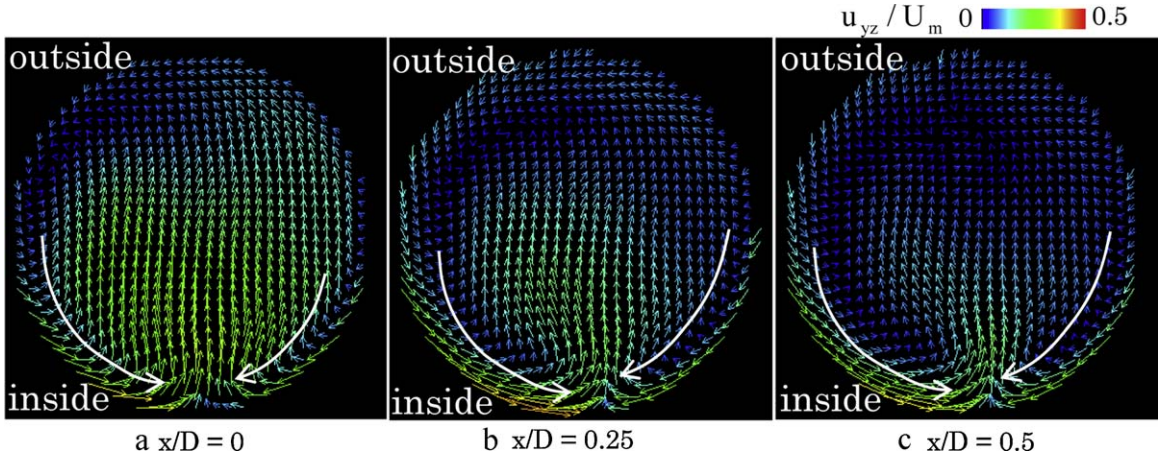

Fig. 17. Time-averaged velocity fields in the cross-section of the pipe (long-elbow case).

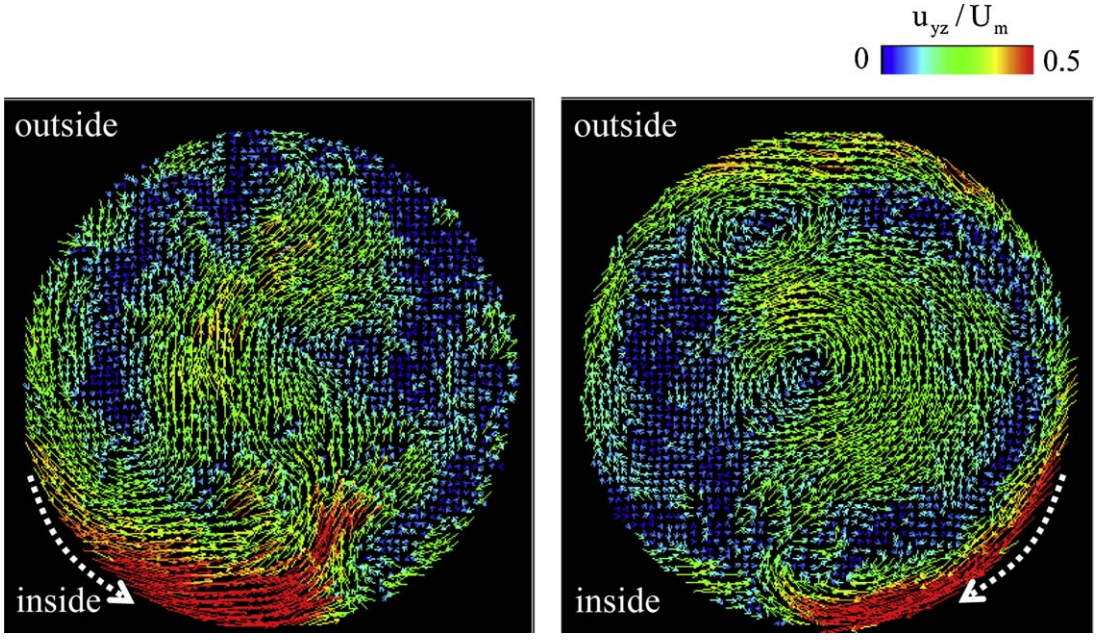

Fig. 18. Time-series velocity fields in the cross-section of the pipe (short-elbow/high velocity case).

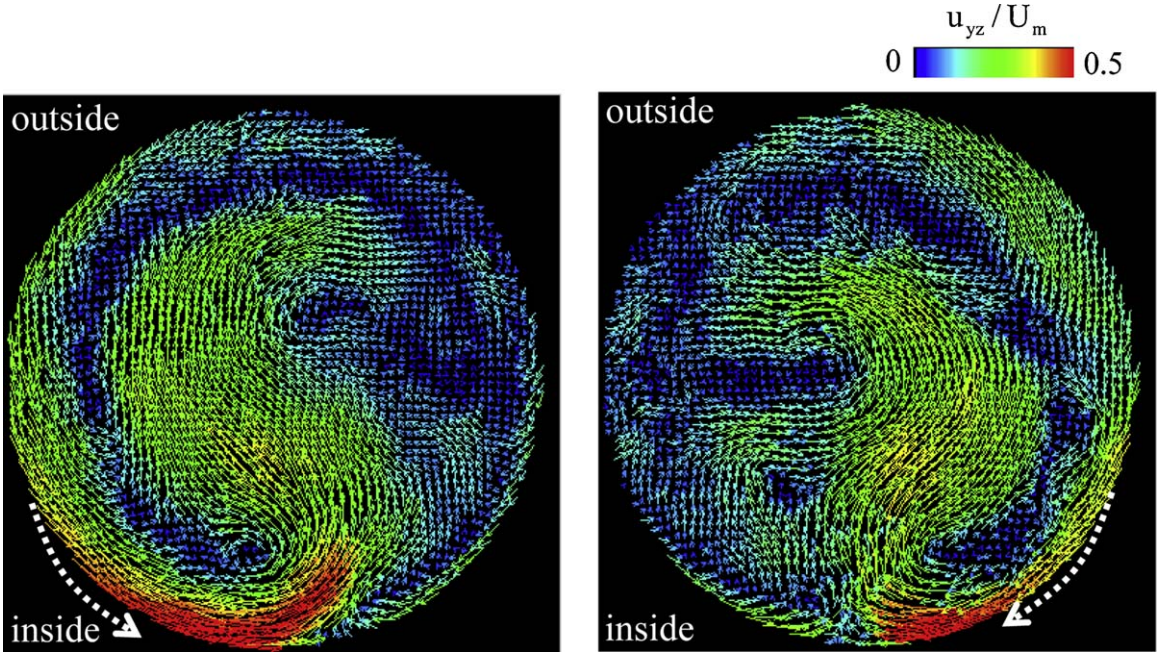

Fig. 19. Time-series velocity fields in the cross-section of the pipe (long-elbow/high velocity case).

from lateral side to inside were observed along the wall as the secondary flow. When the high velocity axial flow reached the outside wall, this flow was changed from outside to lateral side of pipe and flowed in clockwise and counterclockwise directions. Fig. 16(b) and (c) shows the flow patterns at the downstream of the reattachment point ($x/D = 0.27$). It was found that the circumferential secondary flow developed downstream of the reattachment point. The acceleration phenomenon also occurred downstream from this reattachment point as mentioned in Section 3.2. These circumferential secondary flows toward the inside wall shown in Fig. 16(b) and (c) will bring higher momentum in main flow direction into the inside wall region. Thus, the circumferential secondary flow induced the acceleration phenomenon near the wall. Fig. 17 shows the time-averaged velocity fields in the pipe cross-section at $x/D = 0$, 0.25 and 0.5 in the long-elbow. The circumferential secondary flow was seen in all the cross-sections. The acceleration phenomenon in the long-elbow case occurred at closer downstream from $x/D = 0$, where the circumferential secondary flow developed. Therefore, it was found that also in the long-elbow case, the acceleration phenomenon was caused by inflow of circumferential secondary flow.

Figs. 18 and 19 show the time-series of velocity fields in the cross-sections at $x/D = 0.5$ in the short-elbow and at $x/D = 0.25$ in the long-elbow. The time-averaged velocity field was nearly symmetric in the cross-sections. However, the time-series data showed that the circumferential secondary flow in clockwise and counterclockwise directions flowed toward the inside wall alternately. This alternate circumferential secondary flow would cause fluctuation of the flow structure including the flow separation near the inside wall of the elbow.

4. Conclusions

The water experiments with two types of 1/8 scaled elbows with different curvature ratio, $r/D = 1.0$, 1.5, were conducted. The velocity fields in the elbow were measured using a high-speed PIV method with high time resolution at $Re = 1.8 \times 10^5$ and 5.4×10^5. The conclusions obtained in this study are summarized as follows:

(1) The separation region in the short-elbow was generated constantly. On the other hand, the separation region in the long-elbow was formed intermittently.
(2) The acceleration phenomenon occurred near the inside wall just downstream of the reattachment point of flow separation. This local acceleration phenomenon was caused by the secondary flow which flowed into the inside wall along both lateral sides.
(3) The circumferential secondary flows in clockwise and counterclockwise directions flowed toward the inside wall alternately and this periodical inflows would affect the behavior of separation region near the inside wall.

Acknowledgements

The authors would like to thank Mr. Ito, Mr. Sekine and Mr. Seki of Joyo Industry Co. Ltd. for conducting this study together with us.

References

Bovendeerd, P., Steenhoven, A., Vosse, F., Vossers, G., 1987. Steady entry flow in a curved pipe. J. Fluid Mech. 177, 233–246.
Eaton, J.K., et al., 1979-7. Proc. 2nd Symp. Turbulent Shear Flows, pp. 16.7–16.12.
Enayet, M.M., Gibson, M.M., Taylor, A.M.K.P., Yianneskis, M., 1982. Laser-Doppler measurements of laminar and turbulent flow in a pipe bend. Int. J. Heat Fluid Flow 3 (4), 213–219.
Ichimiya, M., Mizuno, T., Kotake, S., 2007. A next generation sodium-cooled fast reactor concept and its R&D program. J. Nucl. Eng. Technol. 39, 171–186.
Idelchik, I.E., 1986. Handbook of Hydraulic Resistance, Second Edition. Hemisphere Publishing Co, pp. 271–275.
Kawamura, T., Nakao, T., Takahashi, M., 2002. Reynolds number effect on turbulence downstream from elbow pipe. Trans. Jpn. Soc. Mech. Eng. B 68 (667), 645–651.
Kotake, S., Mihara, T., Kudo, S., Aoto, K., Toda, M., 2008. Development of advanced loop-type fast reactor in Japan (1): current status of JSFR development. In: Proc. of the 2008 International Congress on the advanced in Nuclear Power Plants, ICAPP'08-8226, Anaheim, USA.
Sakakibara, J., Hishida, K., Maeda, M., 1992. Simultaneous measurements of two dimensional velocity and temperature field using correlation technique and LIF, flow visualization VI. In: Proc. of the 6th Int. Symp. on Flow Visualization. Springer-Verlag, pp. 677–681.
Sandborn, V.A., 1979-7. Proc. 2nd Symp. Turbulent Shear Flows, pp. 4.1–4.5.
Shiraishi, T., Watakabe, H., Sago, H., Konomura, M., Ymaguchi, A., Fujii, T., 2006. Resistance and fluctuating pressure of a large elbow in high Reynolds numbers. J. Fluids Eng. 128, 1063–1073.

Shiraishi, T., Watakabe, H., Sago, H., Kotake, S., Yamano, H., 2008. Pressure fluctuation characteristics of the short-radius elbow pipe for FBR in the postcritical Reynolds regime. In: Proc. of Int. Conf. on Jets, Wakes and Separated Flows, ICJWSF-2008, Berlin, Germany.

Sudou, K., Hibara, H., 1992. Turbulent flow in a circular-sectioned 90° bend. Trans. Jpn. Soc. Mech. Eng. B 58 (548), 1015–1021.

Tanaka, M., Ohshima, H., Monji, H., 2009. Numerical investigation of flow structure in pipe elbow with large Eddy simulation approach. In: Proc. of 2009 ASME Pressure Vessels and Piping Division Conference, PVP2009-77598, Czech Republic.